Journal of Materials Chemistry C

Accepted Manuscript

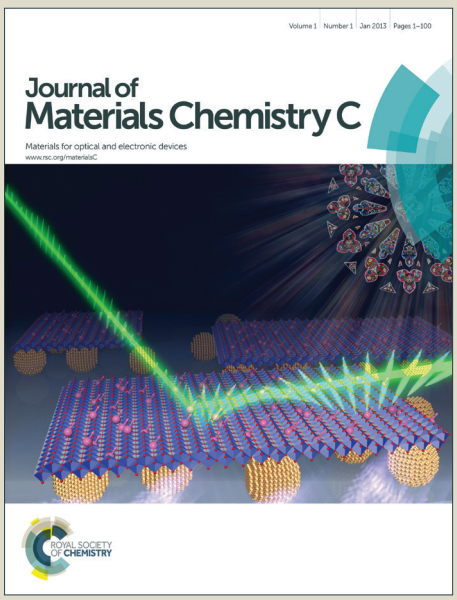

ROYAL SOCIETY OF CHEMISTRY

www.rsc.org/materialsC

Journal of Materials Chemistry C

PAPER

Synthesis, Characterization and Electromagnetic Performance of Nanocomposites of Graphene with α-$LiFeO_2$ and β-$LiFe_5O_8$

Hong Wu,[a] Huifeng Li,[a] Genban Sun,*[ab] Shulan Ma[a] and Xiaojing Yang*[a]

Received 00th January 20xx,
Accepted 00th January 20xx

DOI: 10.1039/x0xx00000x

www.rsc.org/

Face-cantered cubic α-$LiFeO_2$ and spinel β-$LiFe_5O_8$ with uniform size and high dispersion have been successfully assembled on 2D graphene sheets *via* a facile one-pot strategy under different reaction conditions. The reduction of GO by this method is effective and comparable to conventional methods, which was confirmed by X-ray diffraction (XRD), Fourier transform infrared (FT-IR), Raman spectroscopy and X-Ray photoelectron spectroscopy (XPS). The structure of the products can be easily controllable by changing the solvent and reaction temperature. It was shown that the as-formed β-$LiFe_5O_8$ and α-$LiFeO_2$ nanocrystals with a diameter of *ca.* 5 nm and 7 nm, respectively, were densely and uniformly anchored on the graphene sheets, and as a result the aggregation of the nanoparticles was effectively prevented. The investigation of the microwave absorbability reveals that the α-$LiFeO_2$/GN and β-$LiFe_5O_8$/GN nanocomposites exhibit excellent microwave absorbability, which is stronger than the corresponding α-$LiFeO_2$ and β-$LiFe_5O_8$ nanostructures, respectively.

Introduction

With tremendous progress in absorbing stealth technology, much effort has been devoted to the fabrication of new high-efficiency electromagnetic (EM) microwave absorbing materials that possess a high reflection loss, broad bandwidth, thin thickness and light weight.[1, 2] Lithium ferrites, especially $LiFeO_2$ and $LiFe_5O_8$, as one of the most promising representative iron-based materials, with the advantage of low cost and environmental friendliness,[3] have been extensively studied for various technological applications, such as microwave devices,[4] optical isolators,[5] ferrite-core memory systems,[6] and cathode/anode materials in rechargeable Li-ion batteries.[7-11] For the electromagnetic wave absorbing field, $LiFe_5O_8$, as one of soft magnetic materials, possesses the advantages of extremely high Curie temperature, square hysteresis loop, low eddy current losses and light weight.[12, 13] However, the products were obtained only with the uneven particle sizes of *ca.* 10 nm to 5 μm by a variety of methods such as flash combustion,[14] sol–gel,[15] citrate precursor,[3, 6] coprecipitation[16] and conventional standard ceramic technique.[12] Jovic et al have successfully prepared small grain sizes in the range of 10 to 20 nm using a modified combustion method with citric acid as a fuel for combustion reaction. But through this route, nanoparticles were reunited together easily.[3] As we all know, the size and geometrical morphology will affect wave absorption performance.[17] Nevertheless, nanoparticles, especially magnetic nanoparticles, are very easy to aggregate together due to their magnetic properties and Van der Waals forces. Hence, a key for the synthesis of absorbing nanomaterials with excellent EM wave absorption performance is to prevent the agglomeration and obtain monodisperse nanoparticles in the matrix.

On the other hand, $LiFeO_2$ including various crystalline-forms of an α-, β-, and γ-form, layered, goethite-type, hollandite-type, and corrugated layered structures, has been widely reported to be applied as cathode/anode materials in lithium ion battery, because of cheaper, abundance, nontoxic, thermal safety and high capacity.[7, 9-11, 18, 19] Many researchers have previously investigated the electrochemical properties of various crystalline-forms of $LiFeO_2$, especially for α-$LiFeO_2$.[7] The preparation methods of various type of $LiFeO_2$ reported contain solid state reaction, hydrothermal synthesis, ion-exchange, solvothermal synthesis, and low temperature molten salt synthesis.[19] Among the crystalline-forms of $LiFeO_2$, α-$LiFeO_2$ was chosen to study its EM-wave absorption property for its unique structure with lithium and iron atom occupying the same position, which is conducive to having a light weight compared to alloy and iron oxide.

In this work, we were committed to prepare uniform dispersion nanoparticles of $LiFeO_2$ and $LiFe_5O_8$, meanwhile, they were anchored on graphene nanosheets. Hereon, we introduced graphene, not only because the two-dimensional graphene has good electrical properties, but also because graphene is a kind of dielectric loss material, while lithium ferrites are magnetic loss material.[20] Though the α-$LiFeO_2$/MWCNT nanocomposite and porous α-$LiFeO_2$-C composite synthesized by combining a molten salt precipitation process and other methods were reported recently,[7, 10] so far, to the

[a] *Beijing Key Laboratory of Energy Conversion and Storage Materials and College of Chemistry, Beijing Normal University, Beijing 100875, China. E-mail: gbsun@bnu.edu.cn (G. Sun); yang.xiaojing@bnu.edu.cn (X. Yang)*
[b] *Department of Materials Physics and Chemistry, University of Science and Technology Beijing, Beijing 100083, China.*
† Electronic Supplementary Information (ESI) available. See DOI: 10.1039/x0xx00000x

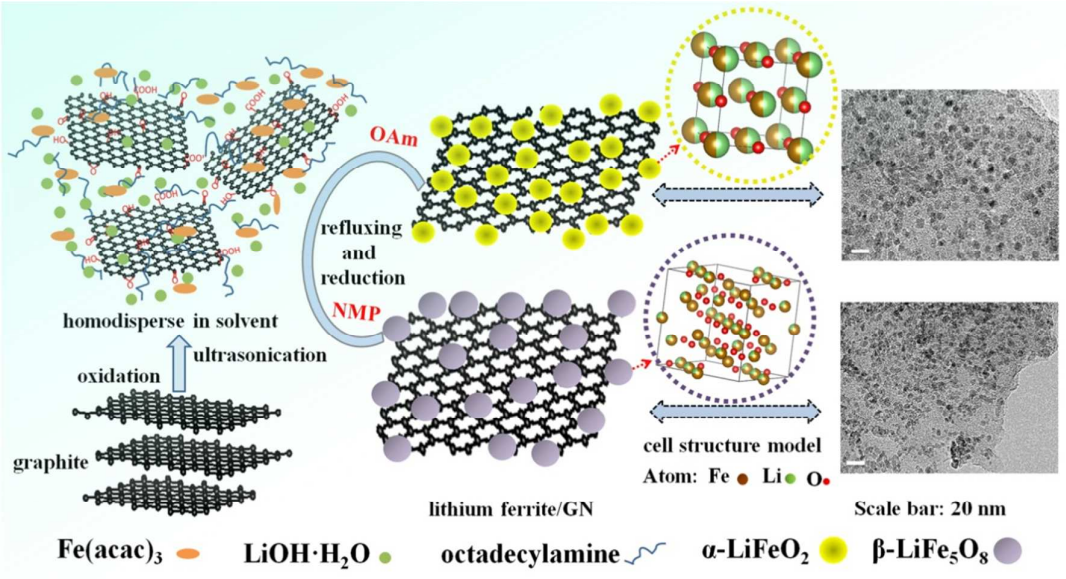

Fig. 1 Schematic illustration of the growth process of α-$LiFeO_2$/GN and β-$LiFe_5O_8$/GN nanocomposites

best of our knowledge, there were almost no lithium ferrite/graphene (Li-Fe-O/GN) nanocomposites reported, which implied it was a challenge to synthesize Li-Fe-O/GN nanocomposites *via* a solution route. Herein, we present a facile one-pot co-thermal decomposition method to synthesize α-$LiFeO_2$/graphene (α-$LiFeO_2$/GN) and β-$LiFe_5O_8$/graphene (β-$LiFe_5O_8$/GN) nanocomposites by simply controlling the reaction temperature and changing the solvent with the same precursors. Furthermore, the two Li-Fe-O/GN nanocomposites exhibit excellent microwave absorbability, which is significantly stronger than the corresponding Li-Fe-O nanostructures.

Experimental section

As illustrated in Fig. 1, the synthesis route is schematically presented. Specific experimental details are as follows.

Preparation of graphene oxide (GO)

GO was synthesized from natural graphite through the modified Hummers' method, which was used as the raw material for the fabrication of Li-Fe-O/GN hybrid.

Preparation of Li-Fe-O/GN nanocomposite

α-$LiFeO_2$/GN nanocomposite were synthesized by a one-pot pyrolysis method. In the first step, 40 mg of GO was added into 40 mL of oleylamine (OAm), and sonicated for 2 h to form a homogeneous brown solution. In the second step, 2 mmol $Fe(acac)_3$, 8 mmol $LiOH·H_2O$, and 2 g octadecylamine were added into the above-mentioned solution, and then the solution was heated to 120 °C and maintained at this temperature for 30 min to remove the moisture in the system, meanwhile, the octadecylamine dissolved. In the third step, the temperature of the solution was increased to 300 °C, and maintained for 2 h. In the fourth step, when the reaction was finished, 20 mL of ethanol was injected into the solution to make the temperature drop quickly. During the first three reaction processes, the reaction system happened in a three-flask with magnetically stirring, and the color of the solution turned from brown to black. In the last step, the final product was separated by centrifugation, washed alternately several times with n-hexane and acetone, and dried at 40 °C under vacuum. Similar to the synthesis of α-$LiFeO_2$/GN nanocomposite, when we employed N-methyl-2-pyrrolidone (NMP) instead of OAm as the solvent, whose boiling temperature is about 202 °C, β-$LiFe_5O_8$/GN nanocomposite was obtained.

Preparation of Li-Fe-O nanoparticles

The method of synthesis α-$LiFeO_2$ and β-$LiFe_5O_8$, agreed with the way to fabricate Li-Fe-O/GN nanocomposites respectively, except for adding GO in the first step.

Characterization

The structures of the samples were recorded by X-ray powder diffraction (XRD) employing a Phillips X'pert Pro MPD diffractometer (Cu Kα, λ = 1.54056 Å) at the room temperature, with a scanning rate of $10°·min^{-1}$, a step size of 0.0167 s^{-1} and 2θ ranging from 10~80°. The generator setting is 40 kV and 40 mA. The further analysis of Li and Fe contents was performed using inductively coupled plasma (ICP) atomic emission spectroscopy (Jarrel-ASH, ICAP-9000). The morphology, size, and microstructure of the as-synthesized samples were investigated by using a field-emission scanning electron microscope (FESEM, acceleration voltage of 5 kV, S-4800, Hitachi) and a high-resolution transmission electron microscope (HRTEM, an acceleration voltage of 200 kV, JEM-2010, JEOL and FEI Technai G2 F20). Atomic force microscopy (AFM) images were taken on

a Brucker Nanoscope III Atomic Force Microscope to measure the height of graphene of the nanocompsits. The samples were prepared by depositing their dispersions on freshly exfoliated mica surfaces and then dried in air before they were measured. Results analyses were taken by Nanoscope Analysis software. Fourier-transform infrared (FT-IR) absorption spectra of the samples were acquired on a Nicolet-380 Fourier-transform infrared spectrometer by KBr method in the range of 400-4000 cm^{-1}. Raman spectra were collected from 800 to 2000 cm^{-1} on a microscopic confocal Raman spectrometer (LabRAMAramis, Horiba Jobin Yivon) using a 633 nm He-Ne laser. X-ray photoelectron spectroscopy (XPS) was carried out on an ESCALAB 250Xi spectrometer (Thermo Fisher) to characterize the surface composition. These products were uniformly blended with paraffin matrix with a mass ratio of 3:2 (60 wt%), and the microwave absorbing devices were prepared with a cylinder shape (Φouter = 7.00 mm and Φinner = 3.04 mm) for the characterization of their EM parameters in the 1.0-18.0 GHz band by employing a vector network analyzer (HP-E8362B, Agilent).

Results and discussion

In this experiment, we chose $Fe(acac)_3$ as raw material, for it can easily form a long-chain organic compound and well generate monodisperse iron oxides nanocrystals. Moreover, some critical factors impact the formation of monodisperse nanocrystals. Firstly, it was necessary to keep the reaction solution at 120 °C for at least half of an hour before it was heated to reflux at 202 °C in NMP or at 300 °C in OAm. In this process, the moisture in the system was removed, while nucleation and growth of nanocrystals slowly happened under these reaction conditions, which can effectively prevent the nanoparticles with wide size distribution formation.[21] Secondly, octadecylamine was also important for the formation of Li-Fe-O/GN, which acted as a surfactant and reductant. Thirdly, in the process of this reaction described in Fig. 1, GO nanosheets with negative charge possess a strong capability to attract the positive charged iron ions and lithium ions through electrostatic force and the actions of bonding because some functional groups, such as -OH and -COOH, were first suspended in the solvent. That is, the GO nanosheet provides a heterogeneous nucleation site and a substrate for the growth of lithium ferrite nanocrystals. Subsequently, the formation of monodisperse lithium ferrite nanocrystals, the reduction of GO nanosheets, and the assembly of lithium ferrite nanocrystals on GN nanosheets occurred *via* the effective in situ route in the presence of octadecylamine. This is similar to the growth mechanism of Co and Ni nanocrystals, which has also been reported in our previous work.[17, 22] In addition, it was worth to mention the significance of solvent in the reaction system. Different solvents tend to form different structures of lithium ferrite. When we used OAm as solvent, α-$LiFeO_2$ nanocrystals were obtained and when solvent was changed to NMP, β-$LiFe_5O_8$ nanocrystals were formed. It is well known that both OAm and NMP belong to organic base and the basicity of OAm is stronger than NMP, because OAm owns amino and double bond. The different basic degree of OAm and NMP may mainly result in different structures of the products. On the other hand, the amount of lithium in the precursor also affected the structure of products. In our experiment, with the increase of lithium content, the products varied from Fe_3O_4 to $LiFe_5O_8$ to $LiFeO_2$ in both solvents. Hence, we can come to a conclusion that alkaline environment and amount of lithium simultaneously contribute to the formation of Li-Fe-O system, and in the reaction system, $LiFeO_2$ and $LiFe_5O_8$ were obtained with lower amount of lithium compared to the general hydrothermal treatments.[23]

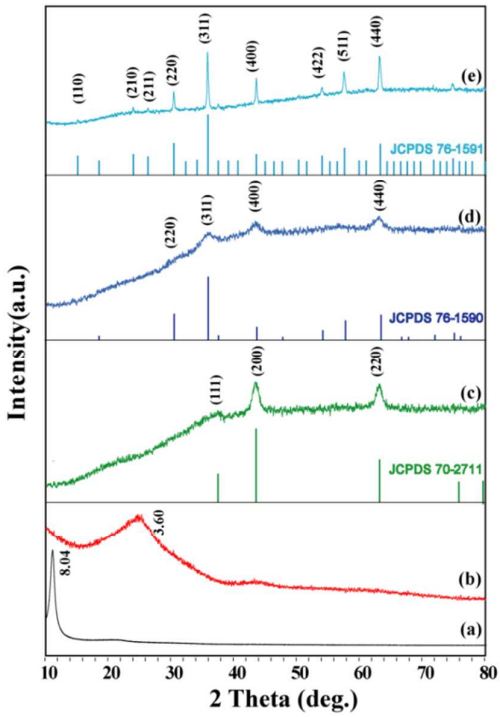

Fig. 2 XRD patterns of (a) GO, (b) GN, (c) as-prepared α-$LiFeO_2$/GN, (d) β-$LiFe_5O_8$/GN nanocomposites and (e) calcined at 700 °C for β-$LiFe_5O_8$/GN.

Fig. 2 shows the XRD patterns of GO, GN, as-prepared α-$LiFeO_2$/GN, β-$LiFe_5O_8$/GN nanocomposites and α-$LiFe_5O_8$ obtained by calcinating β-$LiFe_5O_8$/GN nanocomposite at 700 °C in air. For GO, owing to the oxidation, the basal spacing (d_{basal}) is greatly expanded from 3.35 Å (original graphite)[17, 22] to 8.04 Å (GO), which is belong to the range from 6.5 to 9.0 Å depending on the degree of oxidation.[24] The characteristic diffraction peak appears at around 2θ=10.9°, without the typical diffraction peak of graphite (*ca.* 2θ=26.5°),[17] which confirmed that the oxidation was effective. Fig. 2b gives no clear peaks but only a broad diffraction halo in a 2θ range of 20-30° and a weak peak at 43.2°, which were identified as the lattice planes of (002) and (100) for GN, respectively, indicating that an amorphous carbon structure existed and the GO was well reduced. As for α-$LiFeO_2$/GN nanocomposite (Fig. 2c), three distinct peaks are observed at a 2θ of 37.5, 43.4, 63.1°, which could be ascribed to α-$LiFeO_2$

and are indexed in the face-centered cubic (*Fm3m*) system with lattice parameter a=4.162 Å (JCPDS card no.70-2711), without impurity phase observed. Furthermore, the diffraction peak of GO can't be observed, which possibly resulted from the reduction of GO to amorphous graphene and the stacking of graphene is substantially disordered indicating few layers graphene may be obtained. This phenomenon is identical with the XRD pattern of nanocomposites in Fig. 2d, suggesting that we could get the Li-Fe-O/GN hybrid. As we can see, in Fig. 2d, there are four obvious peaks with a 2θ of 30.5, 35.9, 43.4, 63.0° respectively. All the peaks are consistent with the spinel phase with a cubic space group (*Fd3m*), giving a = 8.292. However, this lattice parameter and XRD pattern are similar to those of three different spinel phases, namely β-$LiFe_5O_8$ (a=8.292 Å), ɤ-Fe_2O_3 (a=8.322 Å) and Fe_3O_4 (a=8.384 Å). In order to further identify the spinel phase obtained, the sample was heated to 700°C in air (as shown in Fig. 2e) and is identified as a single phase of α-$LiFe_5O_8$ ($P4_332$, a=8.314Å). Hence, It was confirmed what we have acquired in NMP solvent was β-$LiFe_5O_8$, because Fe_3O_4, and ɤ-Fe_2O_3 transform to α-Fe_2O_3 at 600 °C and 400-500 °C respectively, while β-$LiFe_5O_8$ transforms to a-$LiFe_5O_8$.[23] Furthermore, the cell structure model of as-prepared α-$LiFeO_2$ and β-$LiFe_5O_8$ are also described in Fig. 1. The β-$LiFe_5O_8$ has a disordered face-centered cubic owning a random distribution of Li^+ and Fe^{3+} ions over the octahedral sites with cations distribution $(Fe^{3+}_2)_{8a}[Li^+Fe^{3+}_3]_{16d}$. As for α-$LiFeO_2$, it has a disordered cubic rock-salt structure with Li^+ and Fe^{3+} ions over the 4a site together.

In order to further demonstrate the composition of the samples obtained, we used inductively coupled plasma (ICP) atomic emission spectroscopy to analyze the contents of Li and Fe. The composition of the α-$LiFeO_2$/GN nanocomposite shows that the Li/Fe molar ratio is 1, while β-$LiFe_5O_8$ nanocomposite approximates 5. As a result, the pure target products were fabricated.

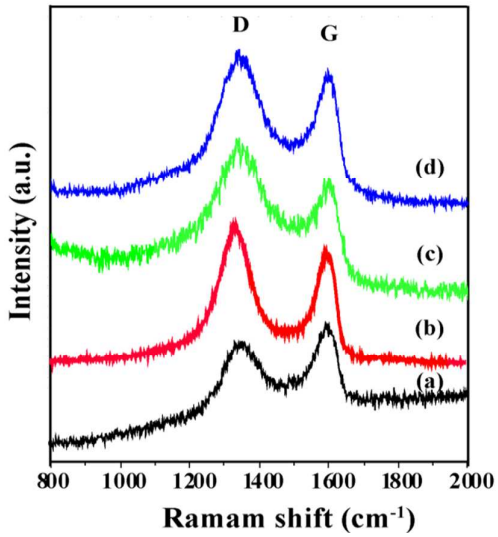

Fig. 3 Ramam spectra of (a) GO, (b) GN, (c) as-prepared α-$LiFeO_2$/GN, and (d) β-$LiFe_5O_8$/GN nanocomposites.

Raman spectra of GO, GN and the as-prepared nanocomposites are shown in Fig. 3 to illustrate the degree of GO reduction. As shown in Fig. 3, the D and G bands of GO are 1348, 1601 cm^{-1}. After reduction, the D and G band of GN, α-$LiFeO_2$/GN and β-$LiFe_5O_8$/GN nanocomposites (1338, 1596; 1344, 1598 and 1343, 1599 cm^{-1}, respectively) are parallel to that of GO, while the ratios of the intensities of two bands (I_D/I_G) are quite different. The intensity ratio of the D and G band (I_D/I_G) is a useful indicator to evaluate the irregular degree and stacking structure.[25] From Figs. 3a-d, we calculated the value of I_D/I_G as 0.96:1 for GO, 1.31:1 for GN, 1.20:1 for α-$LiFeO_2$/GN, and 1.15:1 for β-$LiFe_5O_8$/GN respectively. With the introduction of oxygen functional groups in the process of oxidation graphite to GO, part of the sp^2 carbon atoms changed into sp^3 carbon, contributing to the increase of I_D/I_G. However, compared to GO, the intensities of GN and Li-Fe-O/GN nanocomposites increased obviously. This possibly because the process of reduction GO can result in the stacking degree being reduced and few-layers GN nanosheets formed and that a large-scale of sp^2 carbon atoms appeared in the structures.[26]

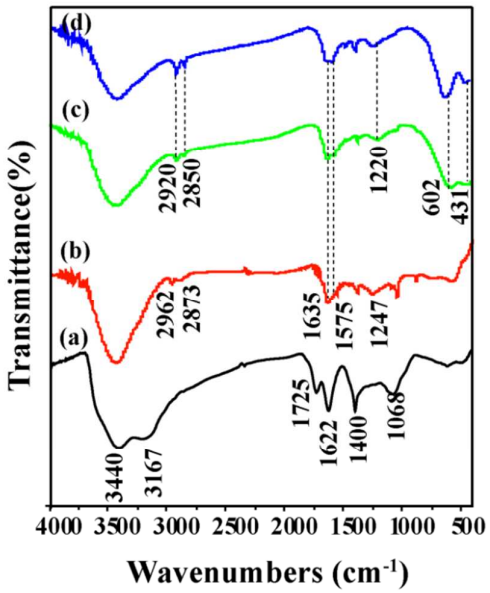

Fig. 4 FT-IR spectra of (a) GO, (b) GN, (c) as-prepared α-$LiFeO_2$/GN, and (d) β-$LiFe_5O_8$/GN nanocomposites.

FT-IR and XPS spectra were further employed to examine the degree of GO reduction. As shown in Fig. 4a, GO illustrates the characteristic absorption bands corresponding to the O-H at 3440 and 1622 cm^{-1} originated from the O-H stretching mode and the stretching deformation vibration of intercalated water, respectively,[22] while O-H at 3167 and 1400 cm^{-1} due to the carboxylic acid.[27] The bond at 1725 cm^{-1} can be assigned to the C=O stretching vibrations in carboxylic derivatives, and carbonyl moieties, while 1068 cm^{-1} is C-O-C (epoxy) stretching vibrations in ether.[28] Compared to GO, in the two as-prepared α-$LiFeO_2$/GN and β-$LiFe_5O_8$/GN nanocomposites, these oxygen-containing functional groups

are distinctly reduced, except for the stretching band of C-OH at 1220 cm^{-1}, which is very difficult to remove in the reduction process of GO. Meanwhile, several new bands at 2920, 2850, and 1575 cm^{-1} emerged (the same with GN in Fig. 4b), which are the alkyl C-H stretching vibration and the aromatic skeletal C=C stretching vibration of GN nanosheets,[29] and the stretching frequency at 602, 431 cm^{-1} are meta-oxygen bonds[30] and these two peaks became widened may result from tiny nanocrystalline particles, large specific surface area, high defects, and low crystal symmetry. Moreover, there remains the absorption of around 1635 cm^{-1}, which still appears in natural graphite,[22] demonstrating that GN with a high purity may be obtained. In addition, the bonds positions in Fig. 4c and Fig. 4d are extremely close. This indicates that the functional groups are similar in these materials. Based on the XPS analysis (Fig. S1, ESI †), we can conclude that a majority of oxygen-containing functional groups, such as -OH and -COOH, in the GO nanosheets have been efficiently removed. In view of the above-mentioned data, we conclude that the GO in the two as-prepared nanocomposites is completely reduced.

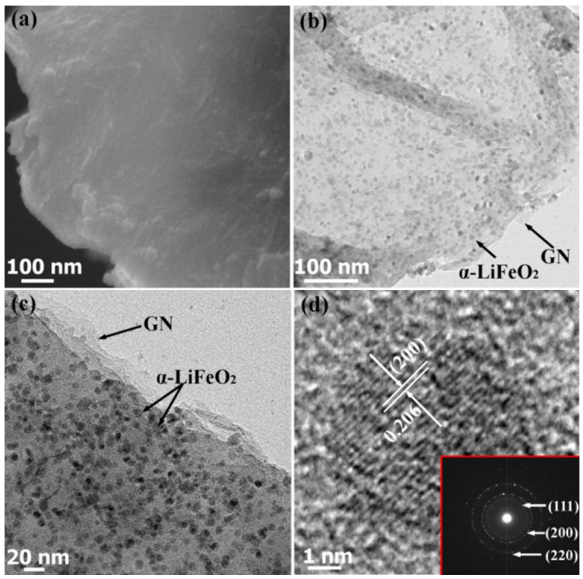

Fig. 5 (a) SEM, (b) TEM, (c, d) HRTEM images of α-$LiFeO_2$/GN nanocomposites. The inset of panel d is the SAED pattern.

To investigate the morphology and structure of the products, the SEM and TEM images of the formed α-$LiFeO_2$/GN nanocomposite are shown in Fig. 5. A general overview SEM image in Fig. 5a shows that a graphene nanosheet anchored with a large number of invisible nanoparticles due to the low-resolution of SEM, which is further more clearly displayed by TEM images. The representative overview TEM images of α-$LiFeO_2$/GN nanocrystals are shown in panels (b) and (c) of Fig. 5. In Figs. 5b-c, a large scale of α-$LiFeO_2$ nanocrystals were successfully fabricated on the two-dimensional GN nanosheets and no agglomeration is observed. As shown in Fig. 5c, α-$LiFeO_2$ nanocrystals are orderly and evenly inlayed into GN nanosheets, indicating that GN can well disperse α-$LiFeO_2$ nanocrystals, even after ultrasonication for TEM characterization. In addition, the outlines of the GN nanosheets and α-$LiFeO_2$ nanocrystals can be clearly distinguished, as well as the nanoparticals are with relatively uniform size of *ca.* 7 nm in diameter. Meanwhile, it is evident that 2D GN sheets have few layers. This possibly confirms that GN nanosheets are well decorated by a large quantity of α-$LiFeO_2$ nanocrystals depositing on their both sides in an orderly, dense manner. Moreover, from Figs. 5a-c, there are almost no separate α-$LiFeO_2$ nanoparticles and GN sheets substrates, indicating that the nanocomposite can be well assembled by the one-pot method. Fig. 5d shows a typical HRTEM image of an arbitrary single as-obtained α-$LiFeO_2$ nanocrystal spreading over the GN surface with a diameter about 6 nm. This presents a clear lattice image, and the lattice spacing is measured to be 0.206 nm, matching the (200) serial plane of α-$LiFeO_2$ nanoparticles in α-$LiFeO_2$/GN hybrid. The selected area electron diffraction (SAED) pattern is shown in the inset of Fig. 5d. The SAED pattern consists of a number of rings, showing that spheres are polycrystallite and all of the ring spots are evaluated to represent d-spacing of 0.237, 0.206, and 0.147 nm, which can be referred to the crystal faces of (111), (200), and (220), respectively. These results can be indexed to cubic phase of α-$LiFeO_2$, which is accordant with the above XRD data.

As shown in Fig. 6, when we used NMP, instead of OAm, as the solvent, simultaneously the second heating temperature changed from 300 to 202 °C, the β-$LiFe_5O_8$/GN nanocomposite can be achieved. From Fig. 6a, we can clearly observed that large-scale tiny β-$LiFe_5O_8$ nanocrystals embedded in graphene in order, which confirms the formation of the β-$LiFe_5O_8$ nanocomposite networks. As shown in Fig. 6b, although not all the nanoparticles are regular sphere compared to α-$LiFeO_2$/GN (Fig. 5c), their sizes are relatively monodisperse, with an average diameter of *ca.* 5 nm. The uniform degree and the dispersibility of nanoparticles prepared through this route are more outstanding than nanoparticles obtained by using macromolecules (such as ethyl cellulose) to control their dispersibility.[5] The 2D lattice fringe image of β-$LiFe_5O_8$ particles formed on GN nanosheets is illustrated in the HRTEM image of Fig. 6c. The lattice fringes with a d-spacing of 0.251 and 0.298 nm could correspond to the (311) and (220) plane, respectively. The SAED pattern also clearly shows a typical polycrystal structure with a few rings in the reciprocal space, suggesting to the crystal faces of (220), (311), (400), and (440), respectively, which is accordant with the above XRD data. To further validate the thickness of graphene in the composite, we used atomic force microscopy (AFM) to characterize the nanocomposite. Figs. 6e and f show typical AFM images of the nanocomposite and the corresponding height analysis profiles, respectively. The sample was dispersed in ethanol solution and formed a uniform dispersion after ultrasonication for a long time. Images were acquired through deposition of the dispersions on freshly cleaved mica substrates. As Fig. 6e displayed, since the ultrasonic time was too long, the particles were scattered and the GN platelet has many concave points,

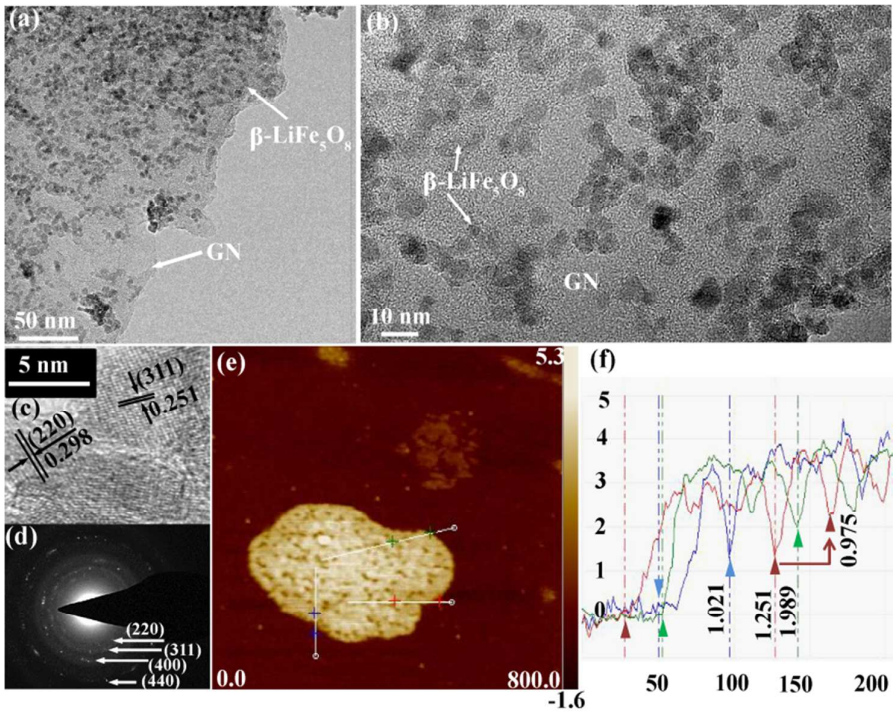

Fig. 6 (a) TEM, (b, c) HRTEM images, (d) SAED pattern and (e, f) AFM images of β-$LiFe_5O_8$/GN nanocomposites and the corresponding height profiles. (unit: nm)

in which nanoparticles grown. On the other hand, we can also accurately measure the thickness of graphene substrates. It reveals that the height of the sample is below 5 nm, and we measured several heights of the concave points, namely 1.021(blue curve), 1.251 and 0.975 (red curve), 1.989 nm (green curve). It suggests that in this system nanoparticles have the possibility to grow on double or monolayer graphene substrates.

To compare and evaluate their microwave absorption properties, α-$LiFeO_2$, β-$LiFe_5O_8$ nanospheres, and their GN nanocomposites were uniformly mixed in a paraffin matrix (60 wt %) which is transparent to electromagnetic waves, and assembled into a microwave-absorption device with an outer diameter of 7.00 mm and an inner diameter of 3.04 mm, and the devices were measured in the range of 1−18 GHz by an Agilent E8362B vector network analyzer. The microwave absorption properties of the as-prepared products can be evaluated by the reflection loss (*RL*) values, which are determined by the relative complex permeability and permittivity on the basis of the theory for microwave transmission, summarized in the following equations.

$$Z_{in} = Z_0\sqrt{\mu_r/\varepsilon_r}\tanh[j(2\pi fd/c)\sqrt{\mu_r\varepsilon_r}] \quad (1)$$

$$RL(dB) = 20\log|(Z_{in}-Z_0)/(Z_{in}+Z_0)| \quad (2)$$

Where *f*, *d*, *c*, Z_0, and Z_{in} are the microwave frequency, thickness of the absorber, light velocity (3×10^8 m/s), air impedance, and input impedance of the absorber, respectively. The results of their microwave reflection losses with different thicknesses are shown in Figs. 7-8.

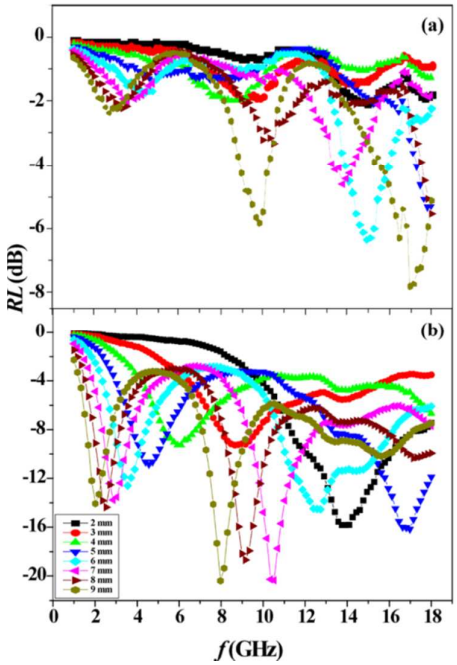

Fig. 7 Microwave reflection losses of (a) α-$LiFeO_2$, and (b) α-$LiFeO_2$/GN nanocomposites with different thicknesses.

The *RL* was measured at a given frequency and thickness. Figs. 7a-b show that the variations of the *RL* values versus frequency for α-$LiFeO_2$ nanospheres and its GN nanocomposite at different thicknesses, respectively. As illustrated in Figs. 7a-b, the absorption position for the two

samples shift toward to lower frequency region and multiple absorption bands (when the thickness is more than 4 mm, there are two absorption bands in the 1.0–18.0 GHz range.) appeared as the absorber thickness of the samples increases. Simultaneously, the thickness also affects the maximum *RL* intensity. Moreover, it is clear that the absorbing performance of GN nanocomposite is obviously superior to pure α-$LiFeO_2$. On the other hand, when the *RL* values of a paraffin-based composite are less than -10 dB, it means that 90% of the EM power is attenuated and only 10% is reflected. And absorbing materials with *RL* less than -10 dB are defined to have great practical application value.[31] The *RL* values for the pure α-$LiFeO_2$ nanoparticles (Fig.7a) cannot reach -10 dB within the thickness range of 1.0-9.0 mm, and the minimum *RL* is -7.8 dB obtained at 16.9 GHz with a thickness of 9.0 mm, which is meaningless for the practical applications. However, as for the α-$LiFeO_2$/GN nanocomposite, when the thickness is 2, 3 and 4 mm, the strongest EM-wave absorption is observed at 13.9 GHz for -16.0 dB, 8.7 GHz for -9.3 dB, and 6.0 GHz for -9.5 dB, respectively; when the thickness is 5, 6 mm, two absorption bands (4.6 GHz for -11.1 dB, 17.0 GHz for -16.4 dB and 3.5 GHz for -12.8 dB, 12.6 GHz for -14.6 dB, respectively) were observed. As the data displayed, the *RL* values less than -10 dB are achieved in the frequency range of 1-18 GHz, while the strongest EM-wave absorption reached -21.0 dB, appearing at both 10.5 and 7.9 GHz, with a thickness of 7 and 9.0 mm, respectively. These results suggest the valuable absorbing characteristic of α-$LiFeO_2$/GN hybrid, which ensures the practical application in wide frequency bands from 1 to 18 GHz by adjusting the thickness of the device.

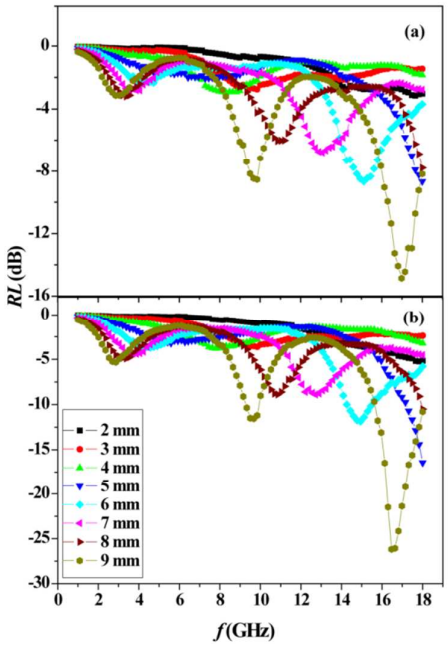

Fig. 8 Microwave reflection losses of (a) β-$LiFe_5O_8$, and (b) β-$LiFe_5O_8$/GN nanocomposites with different thicknesses.

The EM-wave absorption nature of pure β-$LiFe_5O_8$ and its GN nanocomposite are depicted in Figs. 8a-b. As depicted in Figs. 8a-b, the thickness of the sample also plays an important role in affecting the intensity and the position of the frequency at the *RL* minimum. Meanwhile, the microwave absorption performance of nanocomposite is visibly enhanced, compared to the pure β-$LiFe_5O_8$. For pure β-$LiFe_5O_8$, the minimum *RL* is 9.6 GHz, -2.8 dB at the thickness of 3 mm (close to 4 mm) and 18.0 GHz , -8.7 dB at the thickness of 5 mm, while for nanocomposite the minimum *RL* is 9.9 GHz, -3.6 dB; 7.8 GHz, -3.8 dB and 18.0 GHz , -16.7 dB at the thickness of 3, 4, 5 mm, respectively. The strongest EM-wave absorption appears at 16.5 GHz, -26.3 dB, while it is only at 17.0 GHz, -14.9 dB for pure β-$LiFe_5O_8$.

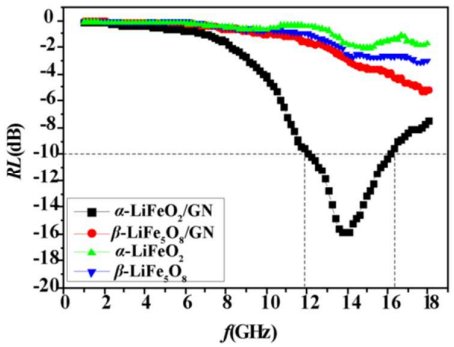

Fig. 9 Comparison of microwave reflection losses of the four as-prepared samples with a thickness of 2 mm.

The wave absorption performances of as-fabricated samples are compared at a thickness of 2 mm in Fig. 9. It is worth noticing the EM-wave absorption of α-$LiFeO_2$/GN is superior to other three samples (> -10 dB). As given in Fig. 9, the minimum reflection coefficient reaches -16.0 dB at 13.9 GHz with an effective absorption bandwidth (< -10 dB) across the frequency range of 11.9-16.2 GHz. On the other hand, as the previous work reported, for pure GN nanosheets, there is almost no EM wave-absorption peak, because the conductive electromagnetic parameters of pure graphene are too high to meet the requirement of impedance match.[22, 31]

In order to explore the possible mechanism of the enhanced microwave absorption of the above α-$LiFeO_2$, β-$LiFe_5O_8$ and their GN nanocomposites, we measured the complex relative permittivity and permeability of the four samples with a thickness of 2 mm, respectively. Fig. 10 shows the real and imaginary parts of the complex relative permittivity (ε' and ε'') and permeability (μ' and μ'') measured for the samples. As shown in Figs. 10a-b, for α-$LiFeO_2$ and α-$LiFeO_2$/GN nanocomposite, the ε' values negligibly decreases from 4.21 to 4.09 and 7.16 to 4.82 in the 1.0–18.0 GHz range, and the ε'' value of α-$LiFeO_2$ increases from 0.07 to 0.19 in the 1.0–18.0 GHz range, while α-$LiFeO_2$/GN exhibits two peaks in the 7.0-11.0 and 12.0–16.0 GHz ranges. Moreover, α-$LiFeO_2$/GN has a higher ε' and ε'' of the permittivity than the other there samples, respectively, which reflects a relative higher dielectric loss and implies an excellent absorbing material with more appropriate conductivity obtained.[31] As for

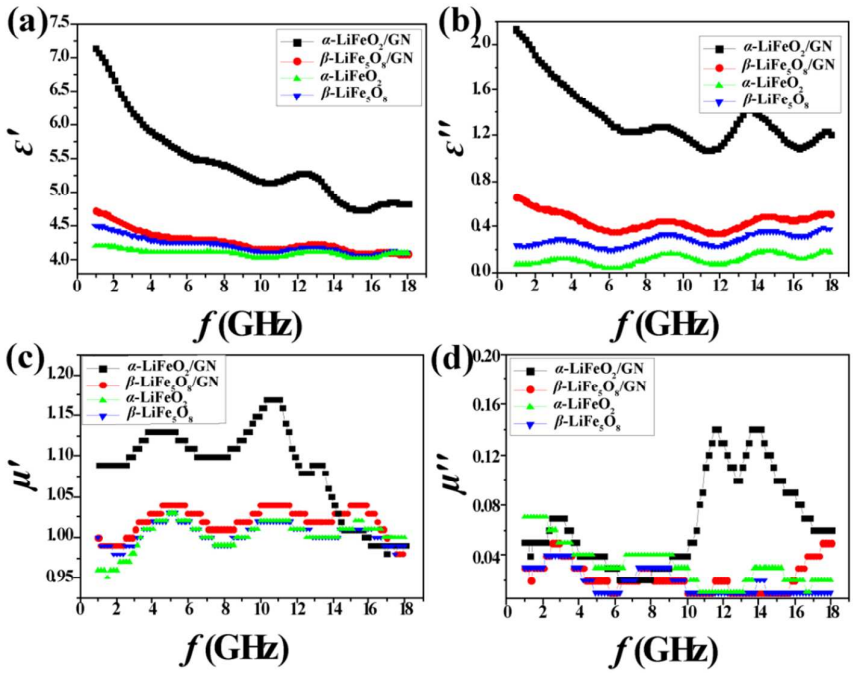

Fig. 10 Frequency dependence of (a) real and (b) imaginary parts of complex permittivity and (c) real and (d) imaginary parts of complex permeability spectra of the four as-prepared samples.

β-$LiFe_5O_8$ and β-$LiFe_5O_8$/GN, the ε' and ε'' values are very low, with negligibly decreasing for ε' from 4.50 to 4.10 and 4.73 to 4.10, and weakly changed for ε'' from 0.24 to 0.38 and 0.66 to 0.51 in the 1.0–18.0 GHz range, respectively. The μ' and μ'' of α-$LiFeO_2$, β-$LiFe_5O_8$ and their GN nanocomposites are relatively stable with frequency increased within the 1.0–18.0 GHz. Meanwhile, the μ'' for the α-$LiFeO_2$/GN composites exhibits a broad resonance peak at 9.8-16.9 GHz. These results show that α-$LiFeO_2$ and β-$LiFe_5O_8$ possess relatively weak dielectric properties and the excellent hysteresis performance, which contribute to the magnetic loss for microwave absorption. However, their GN nanocomposites have better dielectric properties than the pure nanocrystals, respectively.

The results indicate that the values of the complex relative permittivity (ε' and ε'') and permeability (μ' and μ'') for GN nanocomposites are better-matched than pure nanocrystals, indicating there is a resonance behavior, which contributes to the microwave absorption performance. According to the equation (1) and (2), separate α-$LiFeO_2$ and β-$LiFe_5O_8$ cannot achieve the impedance matching conditions, which is also consistent with the *RL* values in Figs. 7-8. Simultaneously, for the impedance match, too high permittivity is also disadvantageous to the impedance match and results in strong reflection and weak absorption.[32] Therefore, to construct favorable microwave-absorbing materials, it is necessary to keep a relatively lower real part of the permittivity and enhance electrical conductivity.[31, 33] For this reason, 2D GN nanosheets are the most adaptive candidate to be introduced. Therefore, it is inferred that dielectric loss and magnetic loss both play an important role in determining microwave properties. The permittivity and permeability mainly originate from electronic polarization, ion polarization, intrinsic electric dipole polarization, interface polarization effect and their magnetic properties, on which the crystal structure, size and special geometrical morphology may have important influences.[17] For example, the enhanced microwave absorption of GN composites mainly results from the following several aspects. The enormous aspect ratio and layered-structure of the composites, the few residual group, defects and Li-Fe-O nanoparticles on GN sheets acting as polarized centers, create multiple reflection.[32, 34-37] Besides, a clear interface and a synergistic effect between the Li-Fe-O crystals and GN matrix (shown in Figs.5-6) favour the interfacial polarization (called the Maxwell–Wagner effect), which occurs in heterogeneous media with large charge at interfaces and dipoles on particles or clusters.[38-40] On the other hand, the microwave absorption properties of α-$LiFeO_2$/GN nanocomposites, are better than β-$LiFe_5O_8$/GN nanocomposites in the low and intermediate frequency, while β-$LiFe_5O_8$/GN nanocomposites are remarkable in high frequency. This phenomenon may be also influenced by the different crystal structures of α-$LiFeO_2$ and β-$LiFe_5O_8$. The former owns a random distribution of Li^+ and Fe^{3+} occupied the 4a site together with the proportion of 1:1, whereas the latter enjoys Li^+ and Fe^{3+} over the 16b site of the octahedral with the proportion of 1:3. Hence, we could conclude that the former may have a stronger motion for Li^+ ions in this structure, along with the synergy of graphene in composites, as the EM wave field, and it is related to a higher dielectric loss of α-$LiFeO_2$/GN nanocomposites. Simultaneously, the quintessential natural resonance and domain wall resonance,

and anisotropic properties of $LiFe_5O_8$ crystals, promote the resonance absorption peak moving to high frequency (shown in Fig.8). There is one more point, should touch on, that the size and dispersion of the nanoparticles on GN matrix may be also crucial factors to enhance the EM absorption performance. With the size decreasing in nanoscale, the number of surface atoms, unsaturated bonds and interface energy would greatly increase, which gives rise to increasing the polarization effect and directly contributes to the dielectric loss.[41,42] Simultaneously, if the dispersion is underdeveloped and nanoparticles conglomerate, the dipole polarization will be weaken, which has been demonstrated in Fe_3O_4 nanoparticles[34]. Accordingly, the high dispersion will conducive to the dielectric loss, thus strengthen the EM absorption performance. On the basis of the above analysis, we can draw a conclusion that in our case the enhanced microwave absorption performance of the GN nanocomposites may be ascribed to the excellent electronic properties of GN nanosheets, special magnetic properties of lithium ferrite nanostructures, and the favourable dispersion of nanoparticles, as well as the different crystal structure between α-$LiFeO_2$ and β-$LiFe_5O_8$.

Conclusions

In summary, a facile method has been successfully developed for the synthesis of α-$LiFeO_2$ and β-$LiFe_5O_8$ nanocrystals evenly embedded in 2D GN nanosheets, with uniform size and high dispersibility. Moreover, it is established that the two kinds of as-synthesized EM absorption materials both own practical application value. In particular, we primarily found α-$LiFeO_2$/GN can be used as a new absorbing material with light quality as well as strong absorption, wide frequency band, thin thickness. The EM wave absorption mechanism of these nanostructures has also been investigated carefully. This work represents a new platform to further study the light quality of lithium ferrite materials, which exhibit a promising prospect as a kind of EM absorbing materials. In addition, due to the magnetic, magneto-optical effect, and elastic properties, the as-obtained β-$LiFe_5O_8$/GN nanocomposites have potential applications in novel magnetic sensors, optical switches and optical isolators, while α-$LiFeO_2$/GN nanocomposites can be used as nanostructured lithium ion battery materials, due to their higher electrochemical activity and theoretical capacity (283 mAh/g).

Acknowledgements

This work is supported by the National Science Foundation of China (NSFC, No. 21271001, 21471020, 51272030 & 21271028) and the Fundamental Research Funds for the Central Universities (No. 2013NT13).

Notes and references

1 L. Wang, Y. Huang, X. Sun, H. J. Huang, P. B. Liu, M. Zong and Y. Wang, *Nanoscale*, 2014, **6**, 3157.
2 N. N. Song, Y. J. Ke, H. T. Yang, H. Zhang, X. Q. Zhang, B. G. Shen and Z. H. Cheng, *Sci. Rep.*, 2013, **3**, 2291.
3 N. G. Jovic, A. S. Masadeh, A. S. Kremenovic, B. V. Antic, J. L. Blanusa, N. D. Cvjeticanin, G. F. Goya, M. V. Antisari and E. S. Bozin, *J. Phys. Chem. C*, 2009, **113**, 20559.
4 S. S. Teixeira, M. P. F. Graca and L. C. Costa, *J. Non-Cryst. Solids*, 2012, **358**, 1924.
5 K. Hayashi, R. Fujilkawa, W. Sakamoto, M. Inoue and T. Yogo, *J. Phys. Chem. C*, 2008, **112**, 14255.
6 S. Dey, A. Roy, D. Das and J. Ghose, *J. Magn. Magn. Mater.*, 2004, **270**, 224.
7 M. M. Rahman, A. M. Glushenkov, Z. Q. Chen, X. J. J. Dai, T. Ramireddy and Y. Chen, *Phys. Chem. Chem. Phys.*, 2013, **15**, 20371.
8 H. Zeng, T. Tao, Y. Wu, W. Qi, C. J. Kuang, S. X. Zhou and Y. Chen, *Rsc Adv.*, 2014, **4**, 23145.
9 K. Y. Li, H. Chen, F. F. Shua, D. F. Xue and X. W. Guo, *Rsc Adv.*, 2014, **4**, 36507.
10 M. M. Rahman, J. Z. Wang, M. F. Hassan, S. L. Chou, Z. X. Chen and H. K. Liu, *Energ. Environ. Sci.*, 2011, **4**, 952.
11 Y. R. Wang, J. Wang, H. T. Liao, X. F. Qian, M. Wang, G. S. Song and S. Q. Cheng, *Rsc Adv.*, 2014, **4**, 3753.
12 V. Verma, V. Pandey, S. Singh, R. P. Aloysius, S. Annapoorni and R. K. Kotanala, *Physica. B*, 2009, **404**, 2309.
13 S. S. Teixeira, M. P. F. Graca, L. C. Costa and M. A. Valente, *Mater. Sci. Eng. B*, 2014, **186**, 83.
14 P. R. Arjunwadkar and R. R. Patil, *J. Alloys Compd*, 2014, **611**, 273.
15 S. Singhal, T. Namgyal, S. Jauhar, N. Lakshmi and S. Bansal, *J. Sol-Gel Sci. Technol.*, 2013, **66**, 155.
16 V. Berbenni, A. Marini, P. Matteazzi, R. Rieceri and N. J. Welham, *J. Eur. Ceram. Soc.*, 2003, **23**, 527.
17 T. T. Chen, F. Deng, J. Zhu, C. F. Chen, G. B. Sun, S. L. Ma and X. J. Yang, *J. Mater. Chem.*, 2012, **22**, 15190.
18 T. Okumura, M. Shikano and H. Kobayashi, *J. Mater. Chem. A*, 2014, **2**, 11847.
19 J. G. Li, J. J. Li, J. Luo, L. Wang and X. M. He, *Int. J. Electrochem. Sci.*, 2011, **6**, 1550.
20 X. Fan, J. G. Guan, Z. Z. Li, F. Z. Mou, G. X. Tong and W. Wang, *J. Mater. Chem.*, 2010, **20**, 1676.
21 S. H. Sun, H. Zeng, D. B. Robinson, S. Raoux, P. M. Rice, S. X. Wang and G. X. Li, *J. Am. Chem. Soc.*, 2004, **126**, 273.
22 G. H. Pan, J. Zhu, S. L. Ma, G. B. Sun and X. J. Yang, *ACS Appl. Mater. Interfaces*, 2013, **5**, 12716.
23 M. Tabuchi, K. Ado, H. Sakaebe, C. Masquelier, H. Kageyama and O. Nakamura, *Solid State Ionics*, 1995, **79**, 220.
24 S. Yang, W. B. Yue, D. Z. Huang, C. F. Chen, H. Lin and X. J. Yang, *Rsc Adv.*, 2012, **2**, 8827.
25 C. F. Chen, T. T. Chen, H. L. Wang, G. B. Sun and X. J. Yang, *Nanotechnology*, 2011, **22**, 405602.
26 J. Su, M. H. Cao, L. Ren and C. W. Hu, *J. Phys. Chem. C*, 2011, **115**, 14469.
27 H. L. Guo, X. F. Wang, Q. Y. Qian, F. B. Wang and X. H. Xia, *Acs Nano*, 2009, **3**, 2653.
28 Y. Si and E. T. Samulski, *Nano Lett.*, 2008, **8**, 1679.
29 C. Nethravathi and M. Rajamathi, *Carbon*, 2008, **46**, 1994.
30 H. L. Kang, M. Leoni, H. M. He, G. L. Huang and X. J. Yang, *Eur. J. Inorg. Chem.*, 2012, 3859.
31 L. Kong, X. W. Yin, F. Ye, Q. Li, L. T. Zhang and L. F. Cheng, *J. Phys. Chem. C*, 2013, **117**, 2135.
32 C. Wang, X. J. Han, P. Xu, X. L. Zhang, Y. C. Du, S. R. Hu, J. Y. Wang and X. H. Wang, *Appl. Phys. Lett.*, 2011, **98**, 072906.
33 P. Bollen, N. Quievy, I. Huynen, C. Bailly, C. Detrembleur, J. M. Thomassin and T. Pardoen, *Scr. Mater.*, 2013, **68**, 50.

34 M. Zong, Y. Huang, Y. Zhao, X. Sun, C. H. Qu, D. D. Luo and J. B. Zheng, *Rsc Adv.*, 2013, **3**, 23638.
35 M. B. Bryning, M. F. Islam, J. M. Kikkawa and A. G. Yodh, *Adv Mater*, 2005, **17**, 1186
36 J. J. Liang, Y. Wang, Y. Huang, Y. F. Ma, Z. F. Liu, F. M. Cai, C. D. Zhang, H. J. Gao and Y. S. Chen, *Carbon*, 2009, **47**, 922.
37 X. Sun, J. P. He, G. X. Li, J. Tang, T. Wang, Y. X. Guo and H. R. Xue, *J. Mater. Chem. C*, 2013, **1**, 765.
38 D. Z. Chen, G. S. Wang, S. He, J. Liu, L. Guo and M. S. Cao, *J. Mater. Chem. A*, 2013, **1**, 5996.
39 P. K. Mandal, A. Lapanik, R. Wipf, B. Stuehn and W. Haase, *Appl. Phys. Lett.*, 2012, **100**, 073112.
40 X. F. Zhang, X. L. Dong, H. Huang, Y. Y. Liu, W. N. Wang, X. G. Zhu, B. Lv, J. P. Lei and C. G. Lee, *Appl. Phys. Lett.*, 2006, **89**, 053115.
41 C. L. Zhu, M. L. Zhang, Y. J. Qiao, G. Xiao, F. Zhang and Y. J. Chen, *J. Phys. Chem. C*, 2010, **114**, 16229.
42 Y. J. Chen, M. S. Cao, T. H. Wang and Q. Wan, *Appl. Phys. Lett.*, 2004, **84**, 3367.

Table of contents

Synthesis, Characterization and Electromagnetic Performance of Nanocomposites of Graphene with α-$LiFeO_2$ and β-$LiFe_5O_8$

Hong Wu, Huifeng Li, Genban Sun, Shulan Ma and Xiaojing Yang**

Monodispersed Li-Fe-O nanocrystals assembled on graphene *via* a one-pot strategy exhibit excellent EM-wave absorbability, stronger than the corresponding Li-Fe-O nanostructures.